ALCATOR C-MOD DESIGN, ENGINEERING, AND DISRUPTION RESEARCH

J. IRBY *Massachusetts Institute of Technology, Plasma Science and Fusion Center Cambridge, Massachusetts 02139*

D. GWINN *Bagley Associates, 7 Bagley Avenue, Lowell, Massachusetts 01851*

W. BECK, B. LaBOMBARD, R. GRANETZ, and R. VIEIRA
Plasma Science and Fusion Center, Massachusetts Institute of Technology Cambridge, Massachusetts 02139

Received March 8, 2005
Accepted for Publication September 26, 2006

We describe some of the engineering solutions required to produce a diverted tokamak capable of operation with a toroidal field of 8 T and plasma currents of up to 2 MA. Some design details of the toroidal field magnet, the ohmic heating magnet, the metal plasma-facing components, the rf heating and current drive systems, and the power and liquid nitrogen cooling systems are discussed. Vacuum, vessel bake, boronization, and wall-cleaning systems are also discussed. Finally, disruption research results from Alcator C-Mod are presented.

KEYWORDS: *tokamak, C-Mod, disruptions*

NOTE: Some figures in this paper are in color only in the electronic version.

I. INTRODUCTION

Alcator C-Mod is a compact, high-field tokamak, with an advanced divertor, molybdenum plasma-facing components, and magnets inertially cooled with liquid nitrogen. Approval to begin the design of C-Mod was given in April 1987, and the first plasma discharges were obtained in October 1992. C-Mod has thus far operated at a maximum toroidal field (TF) of 8.11 T and plasma current (I_p) of 2.02 MA, but the engineering design is qualified for 9-T and 3-MA operation, with disruption field variation rates of 1 T/ms. These high fields and currents, together with the forces expected during full current disruptions, required novel engineering concepts to be developed throughout the design process. A brief overview description of this design as of 2006 is presented. Toroidal field flattops of up to 3.9 s have been obtained at 5 T, but flattop times are reduced to about 1 s at 8 T. These times are long compared to typical plasma L/R times. Shot cycle times, determined primarily by the toroidal field magnet cooldown time, range from less than 12 min to ~30 min at the highest fields. More detailed information can be found in papers from several conference proceedings presented during the design and initial operation phases of Alcator C-Mod.[1–6] Achieved and design machine parameters are shown in Table I.

*E-mail: irby@psfc.mit.edu

II. ALCATOR C-MOD MECHANICAL DESIGN

Figure 1 shows a cutaway view of the Alcator C-Mod vacuum vessel. The Type 304L stainless steel vessel provides the mechanical support for the poloidal field (PF) and ohmic heating (OH) magnets. The vessel is constructed of welded cylindrical and annular components. The innermost cylinder comprising the inner vessel wall was machined to a precision of 0.5 mm and provides support for plasma-facing components and magnetics instrumentation critical to the control of the plasma. The inner wall is 1.5 cm thick at the vessel midplane, but some sections of the vacuum vessel are up to 5 cm thick to provide strength in high-stress regions. There are no toroidal or poloidal electrical breaks in the vacuum vessel, resulting in low toroidal and poloidal resistances of approximately 40 and 10 $\mu\Omega$, respectively. Vessel L/R times range from 20 to 50 ms. A set of 20 gussets at both the top and bottom of the vessel provides additional strength and anchor points for divertor components. A large number of studs provide additional attachment points

TABLE I

Major Machine Parameters for Alcator C-Mod

Major radius (m)	0.68
Minor radius (m)	0.21
Maximum elongation	1.85
Maximum triangularity	0.85
Maximum toroidal field (T)	8.11 (9-T design)
Maximum plasma current (MA)	2.02 (3-MA design)
Plasma volume (m^3)	1
Maximum discharge length (s)	<5
Maximum stored plasma energy (kJ)	250
Vessel volume (m^3)	4
TMP pumping speed N_2 (ℓ/s)	2000
Effective pumping speed N_2 (ℓ/s)	500
Ohmic heating power (MW)	2.7
ICRF source power (MW)	8
Lower hybrid source power (MW)	3
Peak utility power (MW)	24
Peak extracted power alternator/flywheel (MVA)	400 design
Total stored energy alternator/flywheel (GJ)	2

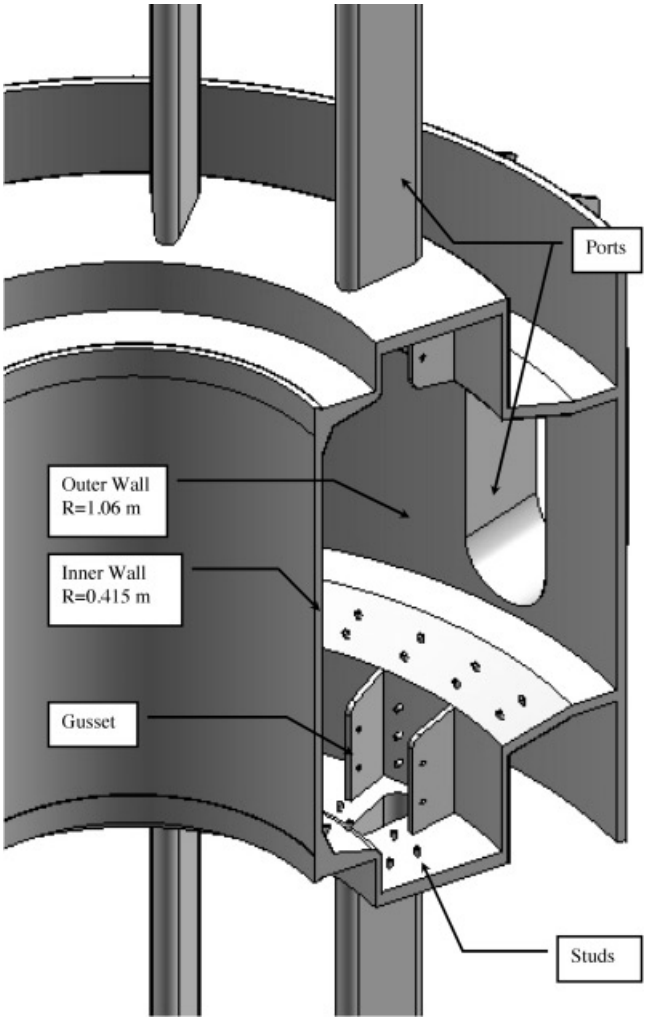

Fig. 1. Cutaway view of the Alcator C-Mod vacuum vessel. The cylindrical and annular components are welded together to form the vessel.

for divertor components, protection tiles, and diagnostics. There are 10 horizontal ports. Nine of these ports are 20 cm wide by 61 cm high. The tenth port, because of extra room needed by the TF bus connection, is only 15 cm wide. The 20 vertical ports are aligned toroidally with the horizontal ones. These ports provide teardrop-shaped access windows that extend approximately 1.5 cm toroidally and 20 cm radially.

Figure 2 shows a cutaway view of the machine. The equilibrium field (EF) coils, EF1, EF2, EF3, and EFC, provide shaping and stability control of the plasma,[7,8] as is discussed briefly in Sec. V. They are secured into pockets formed from extensions of the cylindrical sections of the vacuum vessel with a system of G10 blocks and wedges (G10 is an electrically insulating, glass-reinforced, epoxy-impregnated laminate). The EF4 coils, which supply a large fraction of the vertical field in C-Mod, are supported from the retaining cylinder, as can be better seen in a second cutaway view in Fig. 3 (many of the details from this figure are explained in the following paragraphs). All of the poloidal field coils are symmetrically arranged vertically into upper and lower magnet sets. Stainless steel mounting plates, 3.8 cm thick, cover the pockets and attach to the vessel, clamping the poloidal field coils in place. These mounting plates are keyed into the Type 316LN stainless steel wedge plates that support the toroidal field horizontal arms.

Coaxial current feeds that extend in radially through the cylinder are used for all poloidal field coils except EF4. The feeds are fabricated such that the inner conductor can rotate relative to the outer one. The inner conductor screws into the magnet terminal block with a right-handed thread, and the outer conductor screws into the block with a left-handed thread. When locked together, outside the retaining cylinder, the conductors cannot rotate in either direction without becoming better engaged and more difficult to rotate. Liquid nitrogen flows through the center conductor to cool the coaxial conductor, the terminal blocks, and the magnets.

Fabrication of the EF1, EF2, EF3, and EFC magnets used an electroforming technique to join the magnet terminals to the coil.[9] This process produces a stress-free, high-strength joint with properties comparable to the base metal. Localized annealing of the copper during the more standard techniques of welding or brazing made these processes unacceptable in this application. Epoxy-bonded G10 housings encase the coils and provide liquid nitrogen cooling channels. The turn-to-turn insulation consists of synthetic aromatic polyamide, Dupont NOMEX,

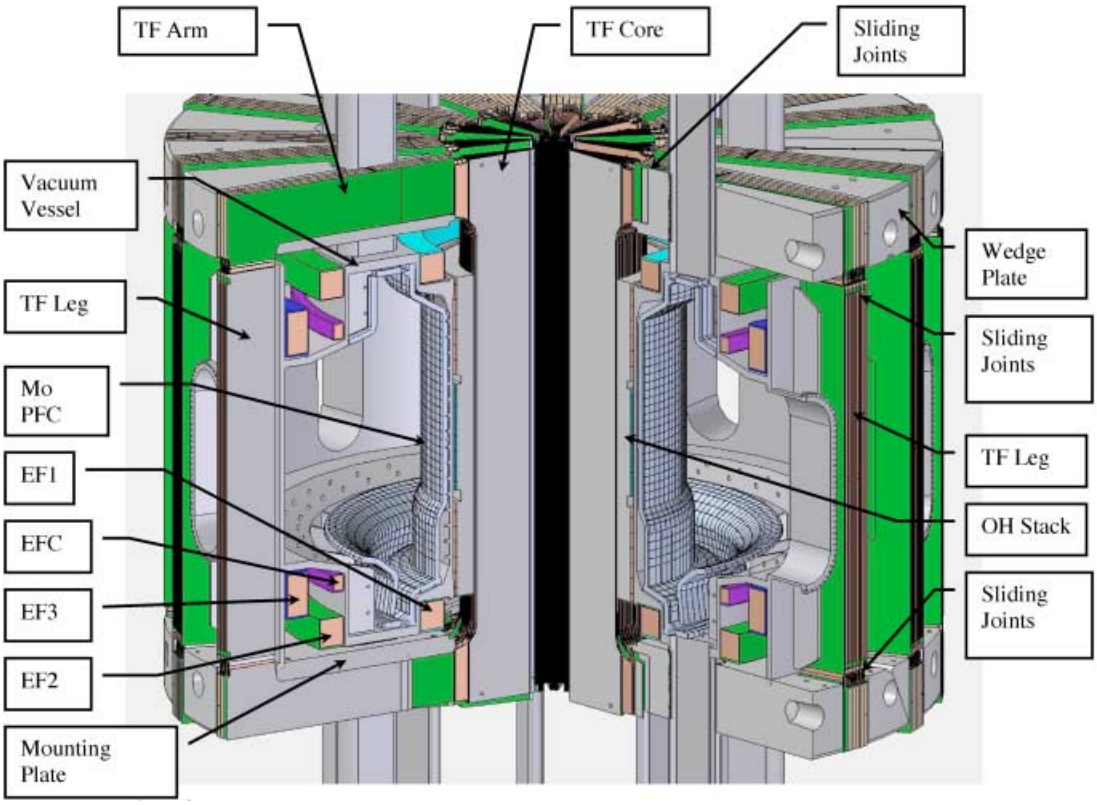

Fig. 2. Cutaway view of Alcator C-Mod. The TF and PF magnets, vacuum vessel, and inner wall hardware are shown. The EF coils are installed in up/down symmetric pairs with labels indicated on the lower coils only. Not shown are the retaining cylinder and domes and the EF4 magnet that attaches to the cylinder.

coated with semicured (B-stage) epoxy that was cured at approximately 150°C.

The current-carrying components of the toroidal field magnet, a six-turn sector of which is shown in Fig. 4, consist of 120 rectangular turns of C-10700 oxygen-free high-conductivity (OFHC) copper with a 250-MPa yield strength. Each turn is made up of four structurally separate conductor plates. Each turn is approximately 180 cm high by 116 cm wide in outside dimensions with a 1.9×18.2 cm^2 cross section. The innermost plates, making up the TF core, are wedge shaped and are bonded together to form a robust cylindrical structure that is adequate to react the local in-plane and out-of-plane electromagnetic loads internally. The TF core copper plates are reinforced by stainless steel plates (Type 216) that keep the copper from yielding under the stresses near the bore region of the core. Spaulrad S insulation (polyamide on woven S glass), 0.762 mm thick, is used between the plates for electrical insulation because of its high compressive strength. Twenty upper horizontal arms, 20 lower horizontal arms, and 20 vertical legs, each made up of six copper plates, form the rest of the TF magnet. A toroidal jog in the plates making up the arms allows for the turn-to-turn progression of the magnet. An epoxy-bonded G10 housing around each arm and leg bundle provides electrical insulation, mechanical strength, and liquid nitrogen cooling paths. The plates are epoxy bonded together with 0.762 mm of G10 insulation between each plate. The in-plane and out-of-plane loads of each bundle are reacted by the heavy stainless steel superstructure.

Forces of up to 110 MN can act to expand the TF magnet vertically against the external superstructure. These forces are first taken up by the upper and lower domes, which then react against the retaining cylinder (see Fig. 3). The domes and cylinder were forged and then machined from Type 316LN stainless steel. This superstructure operates at 77 K, and at this temperature the yield and ultimate strength is more than adequate to carry the applied loads (30 to 40% higher than room temperature values). The domes are 0.66 m thick and 4.9 m in diameter. The cylinder is 0.15 m thick and 2.34 m high. The in-plane loads are carried from the covers to the cylinder by 96 INCONEL® 718 draw bars with a yield strength of 1 GPa. They are pretensioned to 2.2 MN each during assembly. At a toroidal field of 9 T and a magnet current of 250 kA, the domes can deflect as much as 3 mm. Forty INCONEL® 718 taper pins register and secure the wedge plates to the cylinder, and 96 stainless steel dowel pins prevent rotation of the covers relative to the cylinder. The out-of-plane loads on the horizontal

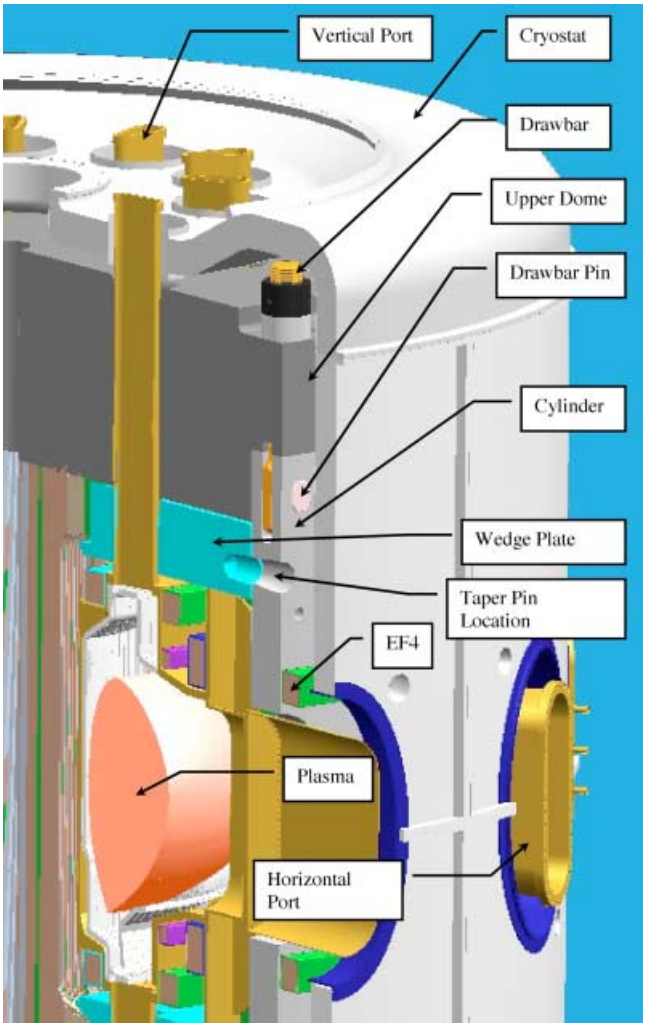

Fig. 3. Cutaway view showing EF4 magnet, cylinder, domes, drawbars, and cryostat.

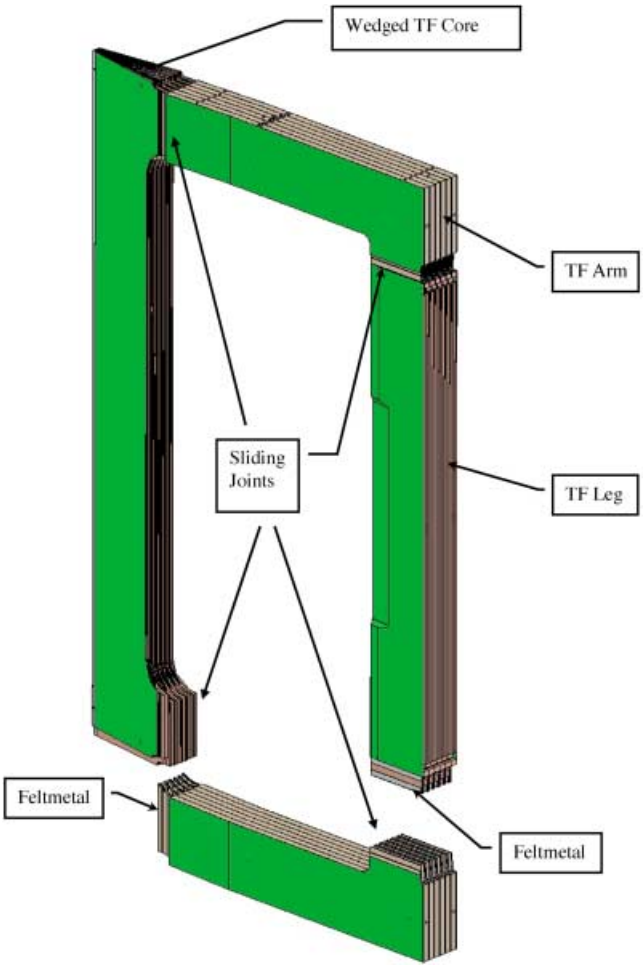

Fig. 4. TF core, vertical legs, and horizontal arms are shown. Also indicated are sliding joint locations.

arm copper plates are reacted through the wedge plates and taper pins into the cylinder. The TF core and arms interlock with slots in the domes to provide additional support for out-of-plane loads.

Because of the very large electromagnetic forces available to both move and distort the TF magnet components, the design of joints that allowed assembly of the magnet was a major focus of the design activity. Figure 5 shows details of a toroidal field magnet sliding joint. These joints allow the TF magnet to always maintain contact with the supporting cylinder and domes. As the joint surfaces move during a discharge, current densities of up to 7 kA/cm^2 must be carried across the joint (magnet current diffusion effects can double the average current density). To carry this current effectively requires the use of a material that can conform well to its mating surface with very low contact resistance. On C-Mod, Feltmetal (from Technetics Corp.) is used to serve this purpose. It consists of chopper-cut copper wire sintered onto a copper substrate to produce a 1-mm-thick pad. The Feltmetal is vacuum baked and silver plated before use. The pads are inductively soldered to the magnet arms and legs. Four pads with a combined area of 72 cm^2 are used for each TF joint. The nominal resistance of each joint is 1.5 $\mu\Omega$ with approximately a ± 0.5 $\mu\Omega$ variation throughout the magnet (includes some finger and plate copper resistance). Springplates are hydraulically driven into position between the TF joint fingers to provide the required contact pressure. The springplates also provide the compliance needed as the joint slides and distorts during normal operation and during disruptions. Force insertion curves are recorded during installation of all 960 springplates, and these data are used to estimate the Feltmetal compression (typically 5.5 MPa). Springplate spacers, either G10 or stainless steel, depending on location, are adjusted in thickness if the compression pressure is found to be out of bounds.

Just prior to installation, the Feltmetal surfaces are coated with colloidal graphite. The graphite provides both

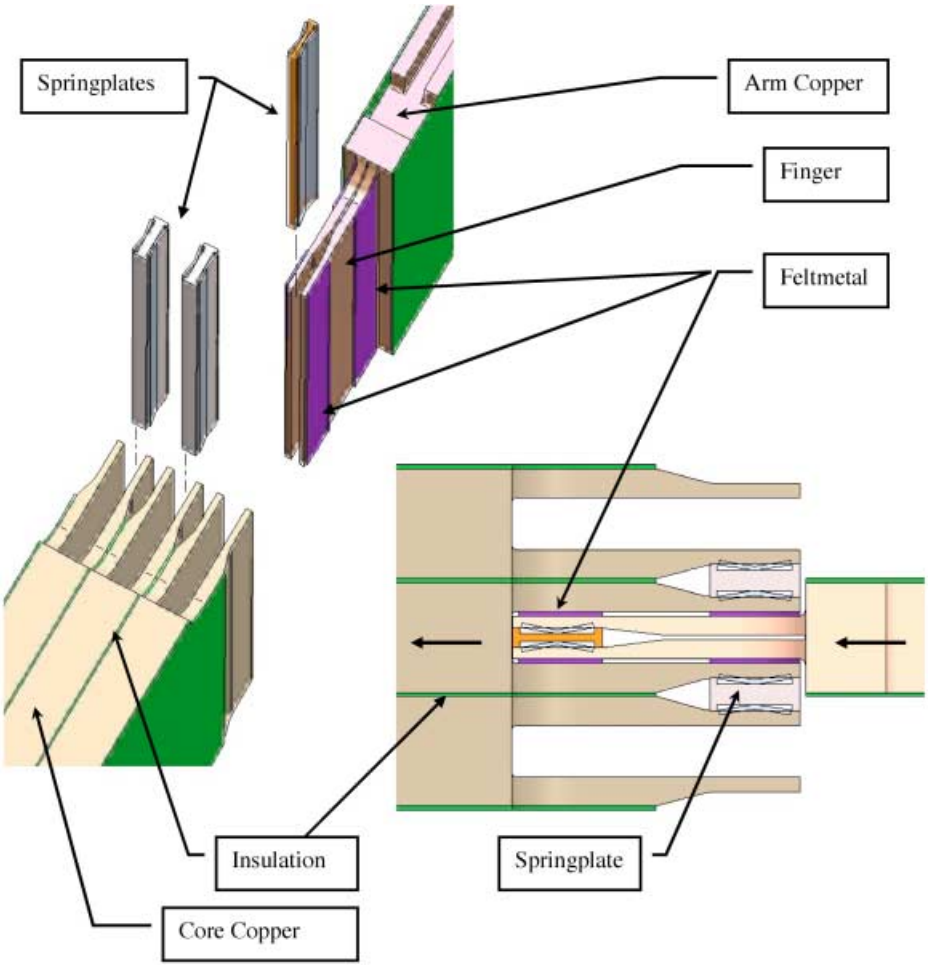

Fig. 5. Details of the TF magnet sliding joints. Four Feltmetal pads provide the low-resistance contacts for up to 250 kA of TF current. The spring plates supply the contact pressure required together with the necessary compliance. The arrows indicate current flow from the arm plate to the core. The dashed lines indicate how the springplates are driven down between the fingers. Only one of the six joints per arm bundle is shown.

immunity to atmospheric gases that can infiltrate the cryostat seals and a lower coefficient of friction for the joint. Sliding tests of uncoated joints cooled to 77 K under the loads expected during operation indicated that the addition of room air, more specifically oxygen, to an otherwise pure nitrogen atmosphere caused rapid failure of the Feltmetal relative to the 50 000-pulse design goal. The application of graphite provided reliable operation of two to three times the design goal. Graphite on similar room temperature joints was first used on the MAST experiment at Culham.[10] During an inspection period beginning in August 2001, the machine was completely disassembled and the entire TF magnet was inspected. All the TF joints were in excellent condition after ~5000 C-Mod shot cycles. Following the inspection, graphite was reapplied to the joints, and the machine was reassembled. Long-term trends in the joint resistances indicate stable operation of the joints since that time.

In Fig. 6, the TF coax used to make the transition from the parallel bus to the first-to-last turn TF vertical leg is shown. The direction of toroidal field current flow is indicated with arrows. Forces not supported in the coaxial structure are reacted against the retaining cylinder. The coax provides a very strong structure through which to conduct the large toroidal field currents. The magnetic field generated by the inner coax conductor is nearly cancelled by the field generated by the outer coax, and nonaxisymmetric field errors are minimized. Two plates, attached firmly with insulated bolts to the cylinder, conduct current from the coax to the first-to-last turn.

TF ripple fields approach 1% near the plasma edge. These fields are time dependent since the current distribution in the TF magnets changes throughout the shot. The single-turn toroidal loop of the TF magnet is uncompensated. Vertical fields of several hundred Gauss can be

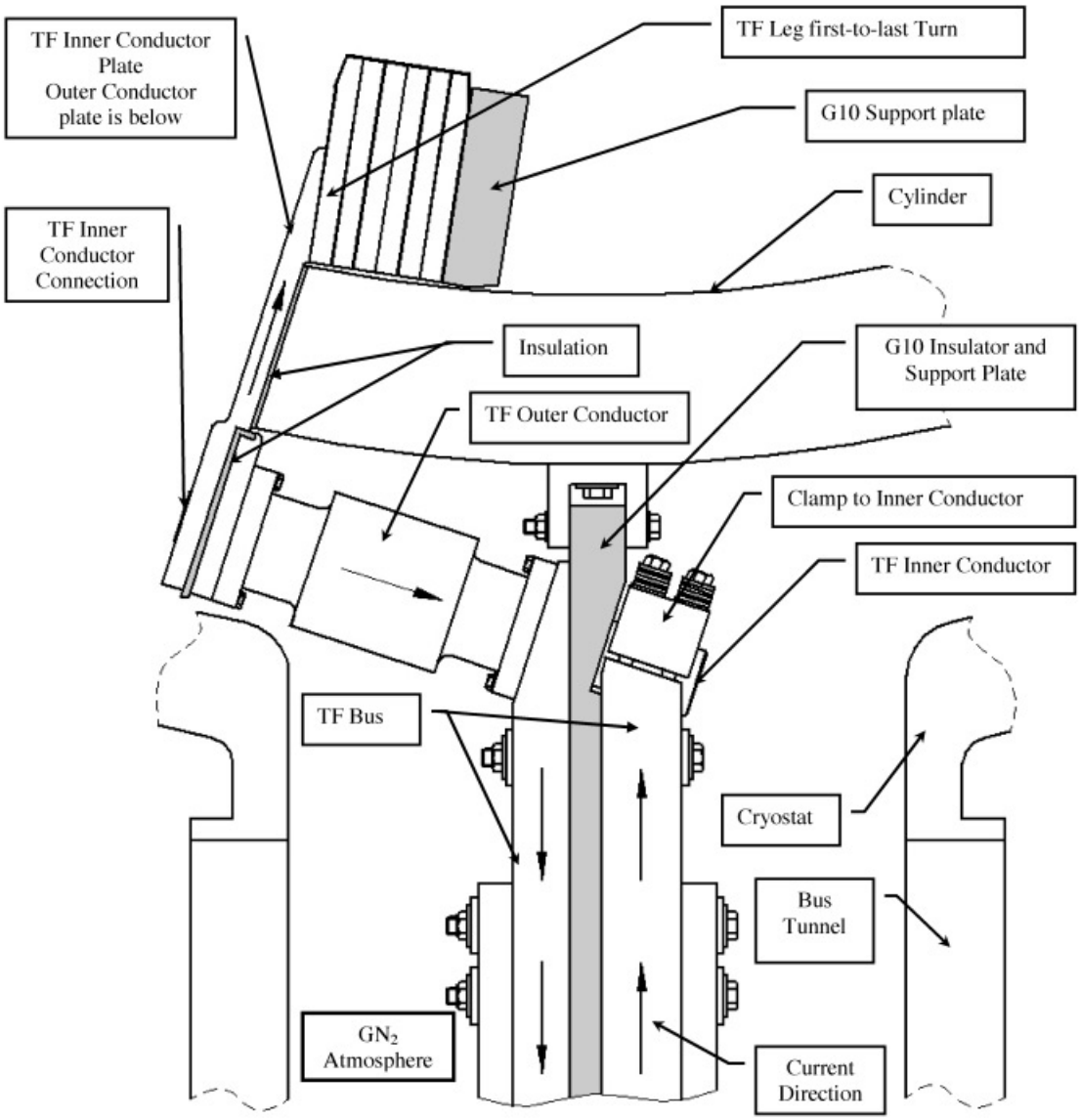

Fig. 6. Current to the TF magnet is supplied by a short coaxial structure that has great strength while minimizing error fields. The arrows indicate direction of current flow. Not shown is the connection from the outer coax conductor plate that runs below the inner plate to the first-to-last-turn connection on the TF leg.

produced near the divertor *x* points from this effect, but the field is toroidally symmetric and compensated by the control system.

A drawing of the OH magnet stack and TF core is shown in Fig. 7. The OH magnet is wound around the TF core but is free to move vertically relative to the core. The OH stack is keyed to the vacuum vessel with a set of mounting blocks that attach to the inner vessel cylinder. A system of pins and Belleville washers ensure proper alignment while allowing movement of the stack over a wide temperature range. Full-hard C-107000 OFHC copper bar with a 16×21 mm^2 cross section is used for all three OH magnets. OH1, with 129 turns, extends the full length of the stack, while OH2U and OH2L, each 27 turns, are wound on the upper and lower one-quarter of the stack on top of OH1. All three coils are visible in Fig. 7. The OH turn-to-turn insulation consists of two half-laps of epoxy-coated Kapton and one half-lap of glass. The OH stack was wound at Massachusetts Institute of Technology and then vacuum impregnated with epoxy.

Up to 30 kA of current (50 kA design) is driven through each of the OH magnets, and the toroidal field can be as high as 17 T at the OH magnet terminals, making this region one of high stress. Coaxial feeds are used to provide current to all three OH magnets. Figure 8

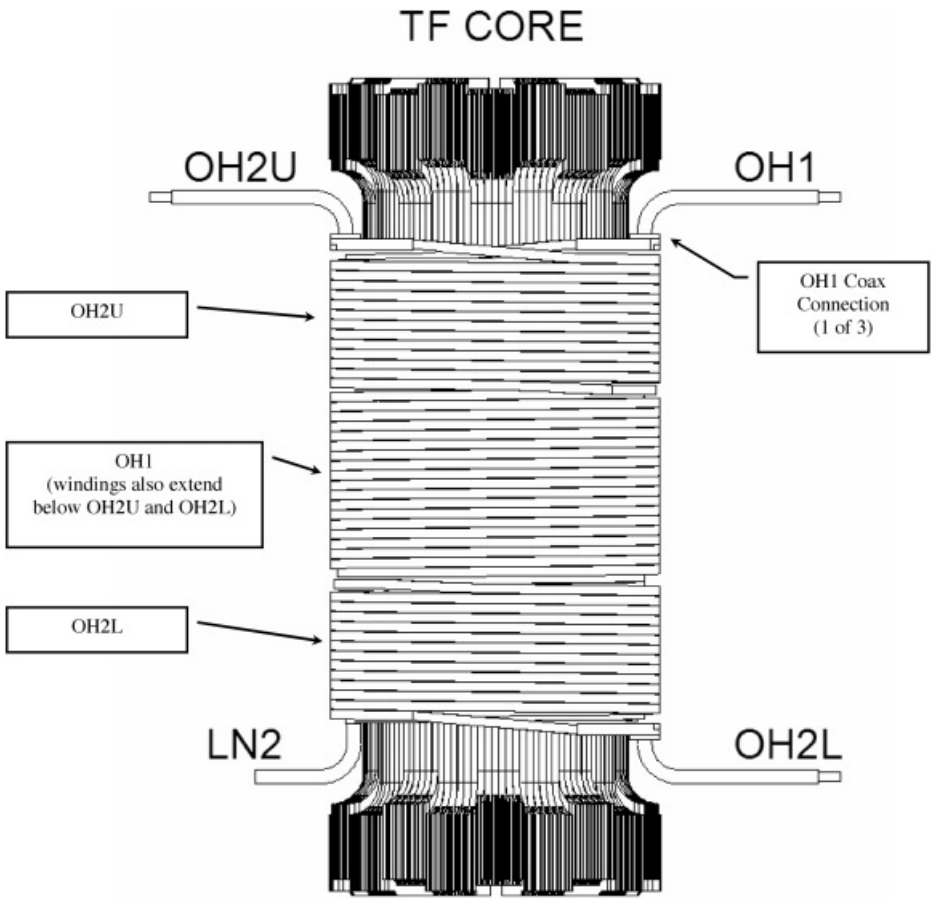

Fig. 7. The OH stack surrounds the TF core. Coaxial connections to all three coils allow reliable 30-kA connections to be made in magnetic fields of up to 17 T. G10 casing insulation around the OH stack is not shown.

shows one of the three assemblies. As with the TF coax, the design allows the forces on the inner and outer conductors to react against each other in a strong structure. Contact to the OH magnet terminal plates is made with Feltmetal pads on both the inner and outer coaxial connections. A unique feature of the design includes a coaxial foot with electric-discharge-machined 25-μm-wide slots that allow the foot to act as a spring. A Belleville washer stack, acting against a stainless steel push rod, compresses the foot against the Feltmetal and maintains contact during a discharge even as the OH terminal pocket moves relative to the feed coax. This design also allows good clamping pressure to be maintained over the large temperature range the joint experiences during cooldown. Overturning forces on the foot required small tolerances on the foot and the pocket into which it slides ($\sim$0.025 mm).

In addition to the primary magnets, eight nonaxisymmetric error field correction magnets, operating at near room temperature, are mounted outside the cryostat on the boron-loaded concrete X-ray and neutron shield. They are located above and below the midplane, at four toroidal locations. These magnets have been used successfully to reduce the effects of locked modes on C-Mod. Error fields on C-Mod arise primarily from the TF bus connection and layer-to-layer radial transitions in the OH1 windings and range up to 0.3 mT in magnitude.[11,12]

III. THE C-MOD DIVERTOR

Parallel heat fluxes as high as 400 MW/m^2, similar to those that will be experienced in ITER, have been measured at the C-Mod outer divertor surfaces during discharges with high levels of rf heating (discussed elsewhere in this issue of the journal). In addition, very large disruption forces generated by both eddy and halo currents have been measured in C-Mod. We briefly describe in this section some of the hardware issues that had to be addressed to reach this level of performance.[13–15] Figure 9 shows a closeup of the lower divertor hardware. Ten stainless steel modules make up the outer divertor. These modules are attached to the vacuum vessel at the vessel gussets via gusset support plates using a set of locating pins to help alignment and Belleville washer

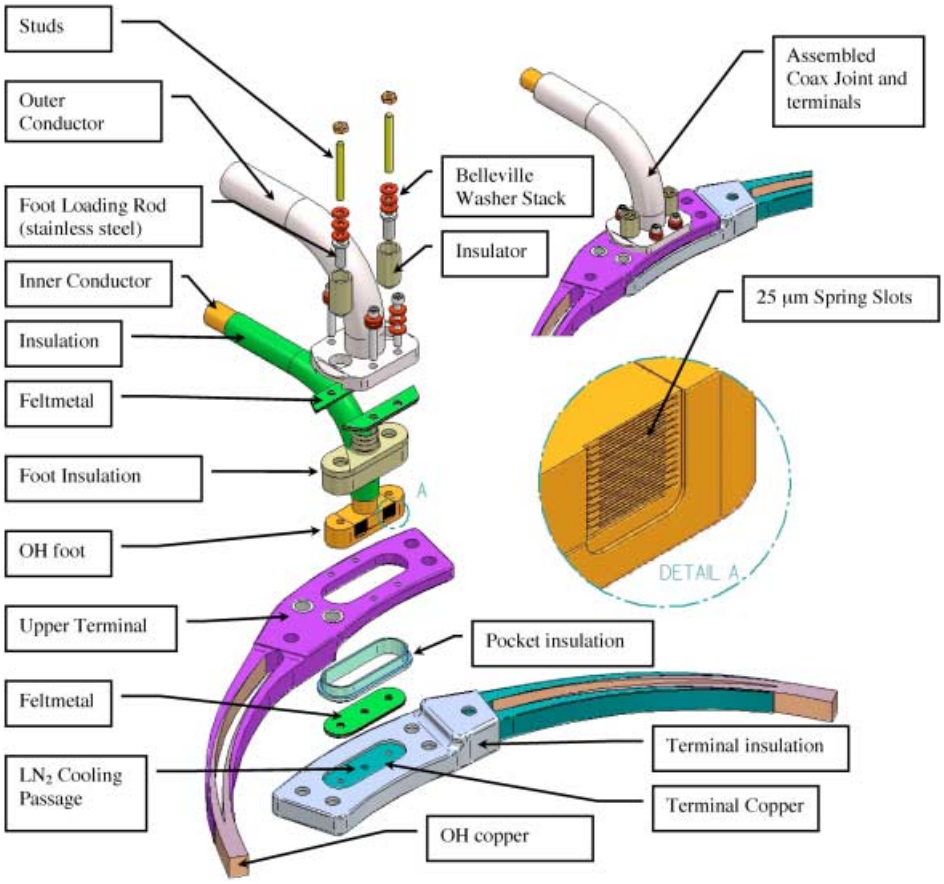

Fig. 8. Details of the OH coaxial connection. Feltmetal pads soldered to both sides of a 1.58-mm copper plate provide a low-resistance connection. Slots machined into the center conductor foot provide additional compliance for the joint. All three OH coaxial connections are of the same design.

stacks to help maintain compression. Each of the 10 outer divertor modules is attached to the gusset support plates by four ceramic-coated INCONEL® 718 pins with spherical bearings. These bearings provide for thermal expansion of the divertor module relative to the vacuum vessel. In addition, the ceramic coating breaks large current loops that would flow through the vessel and divertor modules during a plasma disruption. The modules have toroidal grooves into which alignment bars are placed that then key into the molybdenum (Mo) tiles. This feature prevents rotation of the tiles during disruptions. The tiles are attached to the module with bolts that enter from the back of the module and screw into pins inserted toroidally into the tiles. A similar keying feature is used to secure the inner divertor tiles, as can also be seen in Fig. 9. However, the inner divertor tiles are secured with bolts from the plasma-facing side of the tile. A ramped geometry machined into the tiles reduces the heat load to the tiles at the bolt hole locations by intercepting magnetic field lines that would normally map to the holes. The support for the inner divertor tiles consists of 20 interlocking INCONEL® plates that attach to the inner wall with studs. These plates are silver plated to provide compliance with the inner vessel wall and improve thermal contact. The inner divertor tiles are made out of a three-axis forged TZM (~99.5% Mo, 0.50% Ti, and 0.08% Zr) material with considerably better through-thickness thermal and mechanical properties than the molybdenum tile plate stock used to fabricate the original set of tiles for the outer divertor. The plate stock material in some cases delaminated and fractured in the high–heat load areas during the early operation of C-Mod.

The upper divertor region of the machine has only minimal protection hardware at the present time. Molybdenum tiles surround the upper gussets and ceiling areas. However, this region of the machine will soon be upgraded with a cryopump and new upper divertor hardware.[16,17]

IV. PLASMA-HEATING AND CURRENT DRIVE SYSTEMS

Alcator C-Mod currently has 11 MW of rf source power available for plasma heating and current drive.

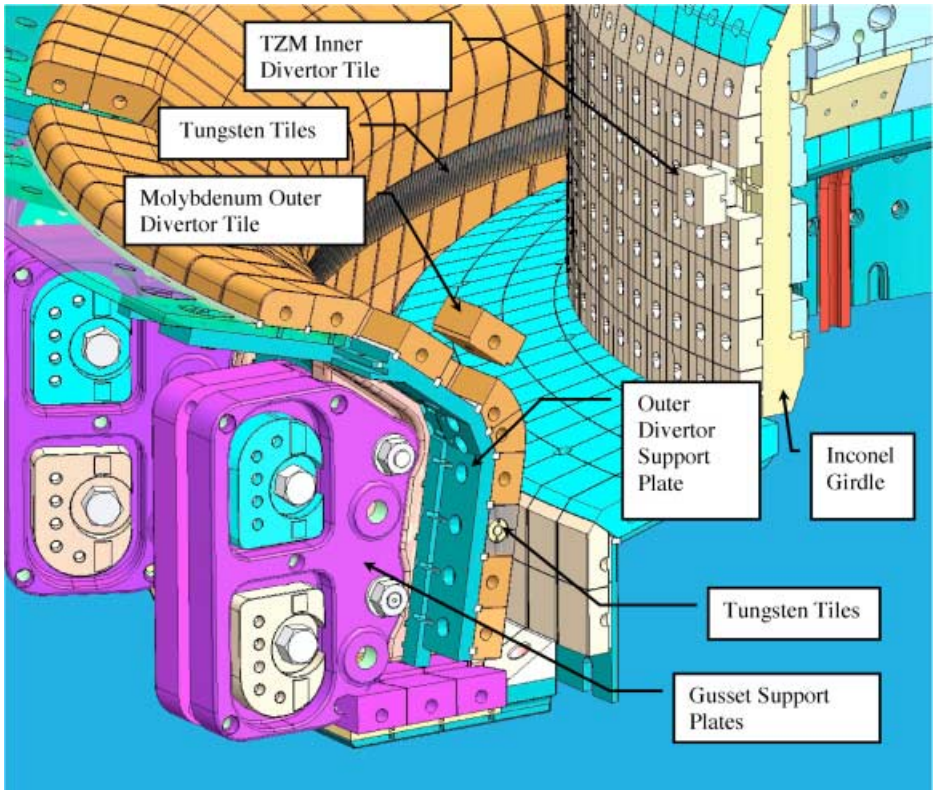

Fig. 9. Details of inner and outer divertor. Tungsten plate tiles yet to be installed in the outer divertor are also shown.

Eight MW of ion cyclotron heating power is provided by four transmitters, each capable of 2-MW cw operation. Two of these systems are tunable from 40 to 80 MHz, while the other two are fixed in frequency at ~80 MHz. These transmitters were originally developed for the Fusion Materials Irradiation Test (FMIT) facility at Los Alamos. These systems drive two 2-strap antennas and one 4-strap antenna, which together have successfully coupled 6 MW of power to the plasma. A picture of the four-strap antenna is shown in Fig. 10. Copper-plated INCONEL® 625 current straps carry the rf currents. The four straps are driven by two transmitters that are phase locked to provide the proper phasing of the antenna for heating or current drive experiments. The Faraday screens for the antennas are also INCONEL®, with either TiC or B_4C coatings. The four-strap antenna uses a Faraday screen with horizontal rods that do not follow the magnetic field pitch. The two 2-strap antenna Faraday screens do approximately follow the field line pitch, but no benefit has been found to aligning the screens with the field lines.

Very recently, 3 MW of lower hybrid source power at 4.6 GHz has become available to support current drive experiments. This system consists of twelve 250-kW cw klystrons powered by a 50-kV, 208-A, insulated gate bipolar transistor (IGBT) regulated power supply.[18] Power is coupled to the plasma through four 24-waveguide couplers, as can be seen in Fig. 11. Molybdenum limiter tiles provide protection for the couplers. The couplers can be moved radially between shots to vary the density at the couplers. A set of Langmuir probes provide essential density information. The klystron amplitude and phase control system allows the relative phases of the 12 klystrons to be changed during a discharge on a fast timescale. $N_{\|}$ can range from 1.5 to 4.5 with the current set of couplers.

Detailed information on the rf systems and rf heating and current drive can be found in Ref. 19.

V. POWER SYSTEMS AND CONTROL

Primary utility power for Alcator C-Mod is provided by a 24-MVA peak power, 13.8-kV line. This line is used to directly power the ion cyclotron radiofrequency (ICRF) and lower hybrid systems, long-pulse diagnostic neutral beam, and the EF2 and EFC magnet supplies. This line also powers the 2-MVA drive motor for the 225-MVA, 14.4-kV alternator and its 65 300-kg flywheel. The flywheel and alternator together store 2 GJ of energy to power the remaining 10 magnet supplies, most of which goes to the TF magnet. During an 8-T, 2-MA discharge, approximately 325 MJ of energy is extracted from the alternator. In total, storage and conversion systems have been designed to supply up to 500 MJ at up to 400 MVA to the experiment.

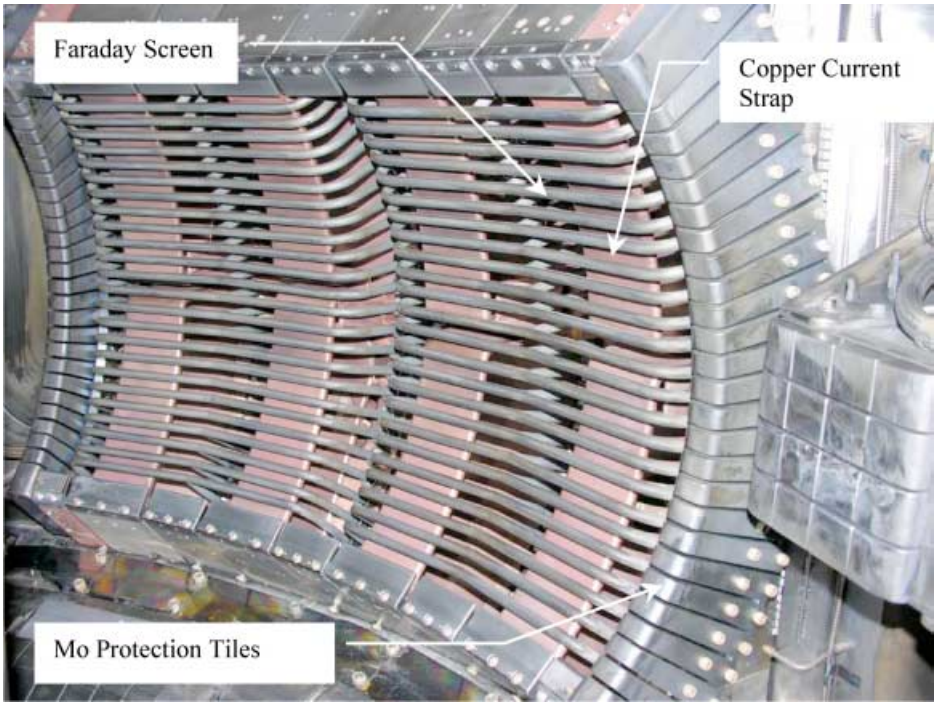

Fig. 10. The four-strap ICRF heating antenna is shown. Up to 3 MW of rf power has been reliability coupled to the plasma using this antenna.

Eleven power converters provide current to the 14 primary magnets (see Table II). All magnets except EF3, EF4, and EFC are driven by their own supply. The EF3 upper and lower coils are driven in series by a single supply. The EF4 upper and lower coils are driven in parallel by a single supply with resistive compensation to equalize currents in the two coils. The EFC supply drives the upper and lower coils in an antiseries configuration.

The low inductance of the EFC coils and a supply capable of generating fast current pulses (chopper) allows this magnet to play a major role in rapid control of the vertical position of the plasma. The OH2U and OH2L magnets provide additional slow vertical position control. The EF3 coils play a major role in controlling the radial position of the plasma, while the EF1 and EF2 coils strongly affect the divertor x-point location. OH2 and EF4 are primary contributors to plasma elongation and triangularity control. The OH1 magnet provides most of the poloidal flux variation needed to drive plasma current, but OH2 and all the EF magnets except EFC also contribute.

The EF1, OH1, and OH2 supply currents are all commutated using a gated silicon controlled rectifier (SCR) switch together with a pulse-forming network to interrupt current flow in the switch. Loop voltages of 5 to 7 V are generated to initiate the plasma discharge. The complex interaction of EF- and OH-produced fields must be carefully tuned to provide the poloidal field null needed for breakdown ($\sim$2 mT). The currents induced in the vessel and superstucture make generation of this null a particularly challenging problem on C-Mod.

The liquid nitrogen–cooled magnets are about a factor of 6 lower in resistance than room temperature magnets. Resistive heating of all the coils, even after accounting for a factor of $\sim$1.6 decrease in the specific heat of the copper, is therefore less of an issue than in water-cooled magnets. During a 5-T, 2-s flattop discharge, the maximum temperature change of the magnets range from 5 to 10°C. The TF magnet bulk temperature during an 8-T discharge will rise 15 to 20°C. During the TF flattop period, the voltage required to drive the TF current is at a lower level because of the lower magnet resistance. During rampdown the inductive energy stored primarily in the TF magnet is returned to the alternator and flywheel.

A digital plasma control system (DPCS) with 128 input and 32 output channels was implemented in 2005 (Ref. 20). Signals from bus Rogowski coils (bus current sensors), magnetic pickup coils mounted on the vessel wall, the two-color-interferometer, and visible bremsstralung detector, among others, go into the DPCS. After processing this information, the DPCS controls power supplies and gas input to obtain the plasma configuration and electron density requested by the operators. The DPCS computer is a Linux-based system running the Interactive Display Language (IDL) to program the control system functionality that allows linear, nonlinear, and adaptive control schemes to be implemented. A Xeon

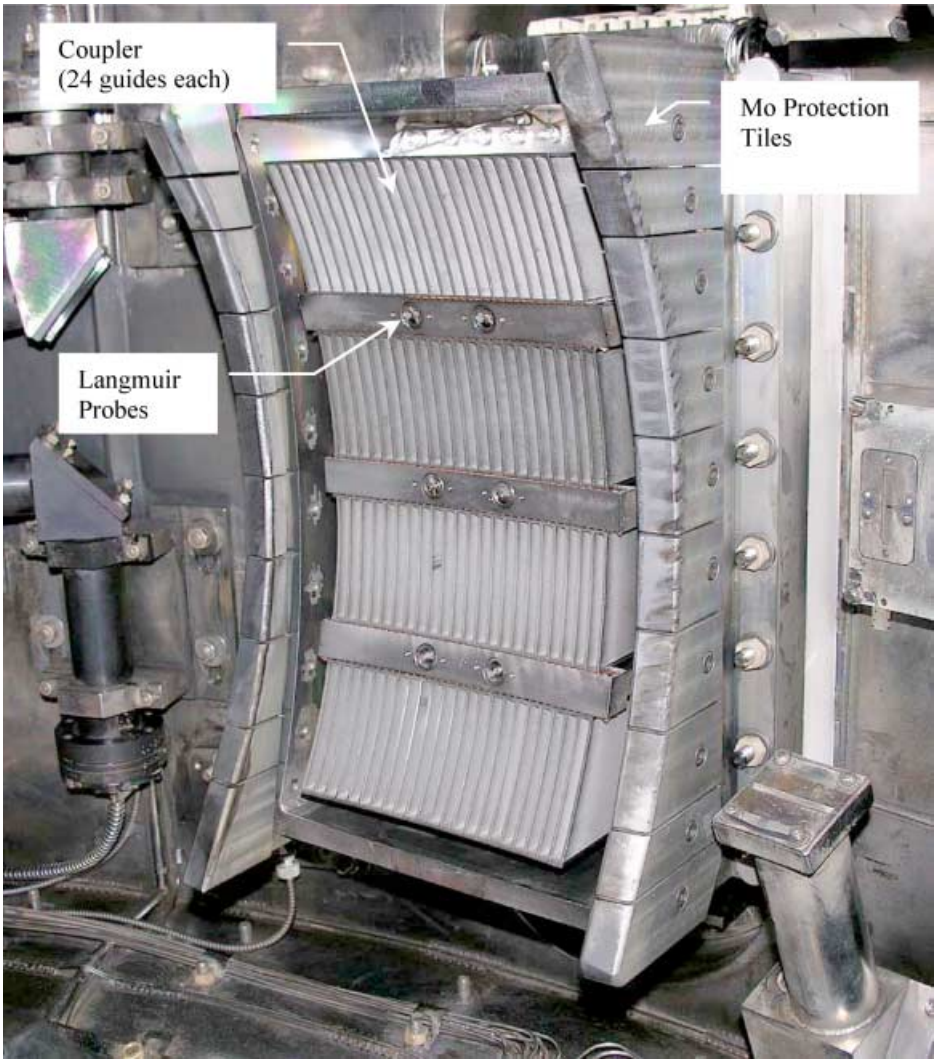

Fig. 11. Four couplers with 24 waveguides each supply lower hybrid power to the plasma. The couplers can be moved radially to match plasma conditions. Langmuir probes between the couplers allow the plasma density to be measured.

3.2-GHz processor with 2 gigabytes of primary memory is used. This system is capable of changing control loop parameters as quickly as once every 100 μs (all input/output lines have the same bandwidth).

VI. LIQUID NITROGEN COOLING SYSTEM

All magnets and supporting structures are cooled with liquid nitrogen. The entire machine is housed inside a cryostat consisting of fiberglass shells enclosing approximately 10 cm of foam insulation (Fig. 3). The cryostat is well sealed against outside air intrusion and maintained at a small positive overpressure of gaseous nitrogen (approximately 300 Pa above atmospheric) to protect the machine from the formation of condensation and ice and to limit access of oxygen to the sliding joint Feltmetal. Liquid nitrogen is supplied from a 73 000-ℓ storage tank at the rate of 32 500 ℓ/day. The nitrogen first fills a 1000-ℓ sump, from which a pump supplies a manifold and valve system that feeds the magnets. The manifold also feeds a cryopanel that cools the upper superstructure. A programmable logic controller (PLC) monitors 60 thermocouples and uses that information to control the supply valves for the TF magnet. Resistance measurements of the other magnets are used to control their cooling. Liquid nitrogen exhausted by the magnets flows to the bottom of the cryostat and then back into the sump, where is filtered and recirculated. Liquid nitrogen boiloff at the bottom of the cryostat effectively cools the lower superstructure.

The TF core is cooled by nitrogen flow both down the central bore of the core and through channels on the outer surface of the core. TF arm and leg bundles are cooled by nitrogen flow between the edges of the copper

TABLE II

Alcator C-Mod Power Convertor Systems

Supply	Output Voltage[a] (V)	Maximum Current (kA)	Additional Comments[b]
Primary Magnet Supplies			
TF	1550/800	260	OV, IOC, crowbar
OH1	932/500	±50	OV, IOC, varistor protection
OH2U	243/100	±50	OV, IOC, crowbar, varistor protection
OH2L	243/100	±50	OV, IOC, crowbar, varistor protection
EF1U	648/492	±15	OV, IOC, crowbar, varistor protection
EF1L	648/492	±15	OV, IOC, crowbar, varistor protection
EF2U	600/500	6	IOC, varistor protection
EF2L	600/500	6	IOC, varistor protection
EF3 (series)	3645/2400	22	OV, IOC, crowbar, varistor protection
EF4 (parallel)	1023/900	±10	OV, IOC, crowbar, varistor protection
EFC (antiparallel)	900/750	3	IOC, varistor protection
EFC chopper	900/750	3	IOC, varistor protection
Commutation Pulse–Forming Systems			
OH2U/OH2L	2kV MAX	50	OV, crowbar protection
OH1	4kV MAX	50	OV, crowbar protection
EF1	2kV MAX	15	OV, crowbar protection
Nonaxisymmetric error correction	600/500	3	IOC, varistor protection

[a]Open circuit/full load.
[b]OV = overvoltage protection; IOC = instantaneous overcurrent protection; crowbar = isolation between supply and magnet during fault conditions; varistor protection = components limit bus voltage by going into conduction as the voltage rises.

plates and the G10 housing. Some of the TF arm cooling exhaust flows directly onto the core sliding joints, giving extra cooling to these critical components.

Liquid nitrogen flows through the OH center coax conductor to directly cool the joints and terminal plates. Nitrogen also flows into a manifold at the base of the OH stack and then upward over the outer surface and back down along the inner surface to cool OH stack conductors. The PF magnets are cooled by liquid nitrogen flow between the edges of the magnets and their G10 housings.

Following any period in which the cryostat has been open to room air, and several days before cooldown, a gaseous nitrogen purge of the cryostat is begun. Liquid nitrogen is not allowed into the sump until the water vapor content within the cryostat drops below 200 parts/million.

VII. MACHINE INSTRUMENTATION

There are 480 sliding joints with 1920 Feltmetal pads on the TF magnet. These are critical locations that are monitored for changes in resistance both between and during discharges. Since both sides of the joints at the TF core are not easily accessible, the two joints at this location are monitored in series, resulting in 360 voltage measurements for the TF magnet. Between discharges, 3 kA of current is driven through the TF magnet and resistance measurements at all 360 locations are recorded. In addition, 16 easily selectable joint locations can be monitored during a discharge with results recorded in computer automated management and control (CAMAC).

The OH coax connections are also monitored. Leads from thermocouples attached to the inner coax foot and the magnet terminal plate are brought back through the inner coax to isolation amplifiers. Both the thermocouple temperatures and the voltage across the contacts are recorded during a discharge. The OH signals are processed following a discharge and alarms are sent to both engineering and physics operators if the signals are out of bounds. The TF signals must be checked by the engineering operator before another shot is allowed.

All magnet currents are measured with Rogowski coils and precision integrators and with a redundant set of shunts. Bus voltages are measured using precision voltage dividers and isolation amplifiers. Several amperes of current are driven through the magnets between shots to monitor magnet resistance and thus average

temperature. All C-Mod magnet supplies have their own set of shunts and voltage dividers to monitor supply performance. The Joule heating to all magnets is monitored (by real-time digital integration of I^2dt) and if allowables are exceeded, the power supply is shut down.

VIII. VACUUM AND WALL-CONDITIONING SYSTEMS

Two 1000-ℓ/s turbomolecular pumps located at a single horizontal port provide the primary pumping system for C-Mod. The effective pumping speed for nitrogen is approximately 500 ℓ/s once relevant conductances are taken into account. Typical base pressures are in the low 10^{-6} Pa range at vacuum vessel operating temperatures of 35°C (maintained by the heater system described below). The vacuum vessel, including port extensions, has a volume of 4060 ℓ. The main chamber has a surface area of about 10 m^2. The horizontal port extension primary seals are racetrack Helicoflex seals. Secondary indium seals provide enhanced leak-checking capability and can also back up the primary seals if a leak develops.

Following a period during which the vacuum vessel has been opened up for maintenance, Alcator C-Mod is baked for several days at a temperature of 130°C. More than 450 resistive foil heaters on a Kapton substrate, monitored by 500 thermocouples, at power levels of up to 100 kW, are required.[21] The coils are cooled to −25°C during the bake to protect the epoxy resin bonding layers, which begin to degrade at 90°C. What might seem to be a rather low magnet temperature was chosen to protect the magnets in the event of a loss of cooling during the bake cycle. The very large thermal mass of the vessel and first-wall components requires several hours to cool down, during which time overheating of the coils, particularly EF1, could occur.

During the bake period, electron cyclotron discharge cleaning (ECDC), usually in deuterium, is applied to clean the vessel walls. ECDC power levels of 2.5 kW at 2.45 GHz are used. The TF magnet current is swept during ECDC to move the resonance from the inner to the outer wall. Sweep times of 120 s are typically used.

The ECDC system is also used for boronization. Diborane gas (usually 90% He, 10% B_2D_6) is metered into the vessel at pressures of approximately 0.8 Pa through a manifold that extends toroidially around the upper part of the vacuum vessel. Because of the high toxicity of diborane, extreme care was given to the design of the boronization system, which can only be operated remotely, with the experimental cell closed to personnel entry. The gas is disassociated in the ECDC discharge, and a boron coating approximately 1200 Å thick is applied over a deposition period several hours long. This process is repeated after about 200 discharges to maintain acceptable plasma performance. Recently, between-shot boronization has been successfully used. Boronization times of ~10 min provide good plasma performance for one or two discharges using this technique. A general discussion of the effects of boronization on C-Mod and the techniques used has recently been published.[22]

Glow discharge cleaning capability is also available. Its primary purpose has been the removal of solid boron compounds deposited on the vessel walls before manned access to the vacuum vessel. A glow discharge in helium breaks down these compounds, leaving a mostly boric acid residue that is completely safe for personnel doing in-vessel work. Two glow discharge electrodes are located in the upper chamber 10 cm away from the vessel wall. Voltages up to 1000 V and currents up to 3 A can be supplied to these electrodes. Ballast resistors can be switched in and out and current and voltages regulated by PLC control. IGBT switches can interrupt power to the electrodes on a timescale short enough to limit damage to vessel surfaces if arcing occurs. These arcs pose no threat to the vessel, but they can sputter stainless steel from the vessel wall onto critical components such as windows, mirrors, and antennas.

Gas for ECDC, glow discharge, and plasma production is provided to the vessel through a set of piezoelectric valves. The voltages to these valves can be controlled by our slow PLC system or by the DPCS. A PLC-controlled manifold system and plena allow gases to be mixed and gas lines to be switched between piezoelectric valves.

IX. DISRUPTION RESEARCH ON ALCATOR C-MOD

Because of Alcator C-Mod's high magnetic field, high plasma current density, and compact size, disruption-induced eddy and halo currents yield much higher electromagnetic forces than those on other tokamaks. Of necessity, Rogowski coils to measure halo currents were installed early in C-Mod's operation, and these led to the discovery and documentation of a large toroidal asymmetry of halo currents.[23] A C-Mod disruption database was established and used to determine scalings of halo current magnitude and toroidal asymmetry as a function of basic plasma parameters, including plasma currents up to 1.5 MA. Much of these data was incorporated into the original ITER disruption database and published as part of the ITER Physics Basis (Chap. 3, Sec. 4).[24] In addition, the empirically derived scalings led to the conclusion that future operation of C-Mod at full performance might produce stresses on the vacuum vessel in the inboard divertor area that would surpass allowable engineering constraints. Therefore, prior to the 2002 run campaign, a major hardware upgrade was installed to strengthen the inboard vessel wall.[14]

During the last several campaigns, a number of experiments have been carried out with the goal of mitigating two of the deleterious effects of disruptions:

1. reducing halo currents to decrease electromagnetic forces on the vessel
2. reducing thermal loading on the divertor strike surfaces by converting plasma energy into light.

Reliable mitigation of these problems using benign techniques would be a key improvement in tokamak operation. However, C-Mod's short disruption timescale poses a difficult challenge for mitigating much of the plasma energy before the usual unstable vertical displacement carries the plasma into the divertor. In principle, it may be possible to significantly delay, or perhaps eliminate, this vertical motion if the plasma is operated at its neutral point equilibrium position.[25] This concept was tested in Alcator C-Mod, and indeed, by operating with the plasma positioned about 3 cm higher than normal (a = 22 cm), the thermally quenched plasma was held for up to 8 ms at the midplane before vertical position control was lost, as shown in Fig. 12. However, during this extended time at the midplane, the plasma current did not decrease significantly, so all the stored magnetic energy was still available to drive halo current when the plasma finally did hit the divertor. Furthermore, the reproducibility of the neutral point behavior was not robust but rather depended sensitively on the particular initial equilibrium.

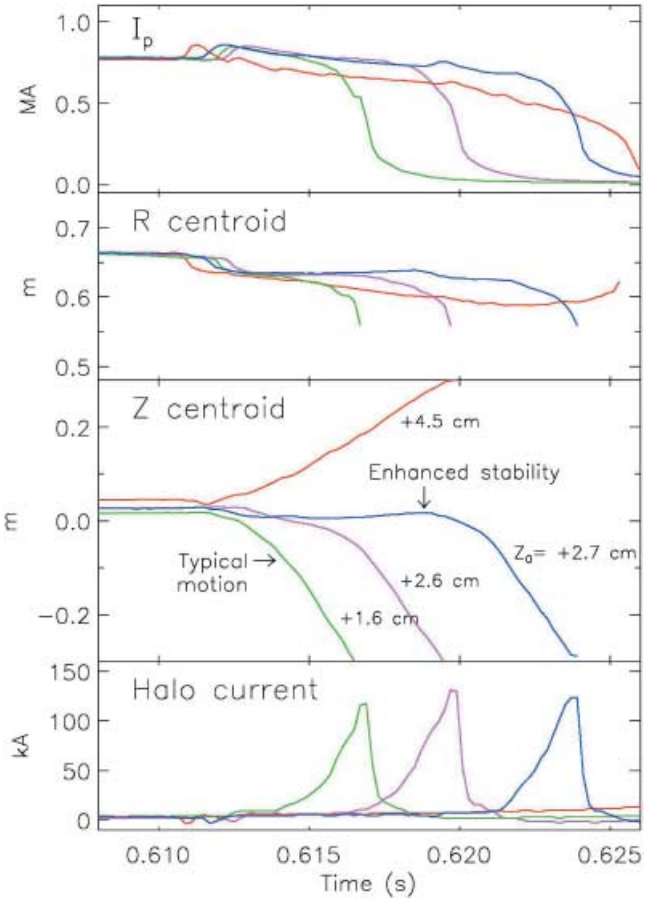

Fig. 12. Disruptions can be delayed by changes in the neutral point location of the plasma. Time histories of the plasma current I_p, the R-Z coordinates of the plasma current centroid, and halo currents are shown. The upward-going disruption halo current was not measured.

Besides electromagnetic forces, it is also desirable to reduce the sudden thermal deposition on divertor surfaces during a disruption, since this can melt or vaporize material in ITER and future reactors. A general method to reduce thermal deposition is to convert a significant fraction of the plasma stored energy (thermal + magnetic) into visible and ultraviolet light by injecting medium- or high-Z impurities, which are efficient radiators. The light is radiated uniformly over the entire vessel interior surface, and therefore the thermal loading is rather benign. Alcator C-Mod presents particularly challenging conditions for thermal energy mitigation due to its short disruption timescale (smaller machines generally have faster quench timescales) and its very high plasma energy density and current density. In fact, the current density in C-Mod is so high that after a typical disruption thermal quench, the plasma reheats to several hundred eV during the subsequent current quench. Empirical results from killer pellet experiments on C-Mod, which employ plastic pellets doped with silver powder, show that the plasma temperature must be reduced to less than 10 eV in order to prevent reheating and that there must be enough impurity species to radiate at a rate of 1 GW. Typical pellet speeds of ~500 m/s were obtained, and pellets usually penetrated all the way to the magnetic axis and often beyond. Pellets were injected radially from the outboard midplane. Several milligrams of silver dopant were required to accomplish this. In these cases, the cold plasma temperature led to a greatly accelerated current quench, less vertical displacement, and reduced halo current in the divertor region, as shown in Fig. 13. Presumably the halo current was reduced because the plasma did not move as far down toward the divertor as normal. In any case, it is generally observed in C-Mod that terminating a plasma quickly by speeding up the current quench reduces the halo current measured in the divertor region. The last trace in Fig. 13 shows that a burst of runaway electrons was generated by the killer pellet. This is extremely rare in C-Mod but is another recognized disruption issue in other tokamaks and is of particular concern for ITER and future reactors because of the potential for localized damage to the wall by the escaping runaway electrons.

A simpler and more reliable way to introduce impurity atoms for disruption mitigation is to use high-pressure inert gas jets. This mitigation technique has been tried successfully in DIII-D (Ref. 26). Experiments to determine the feasibility and effectiveness of this technique in C-Mod plasmas, which have much higher energy density and pressure, as well as shorter disruption timescales, are being carried out with a highly optimized

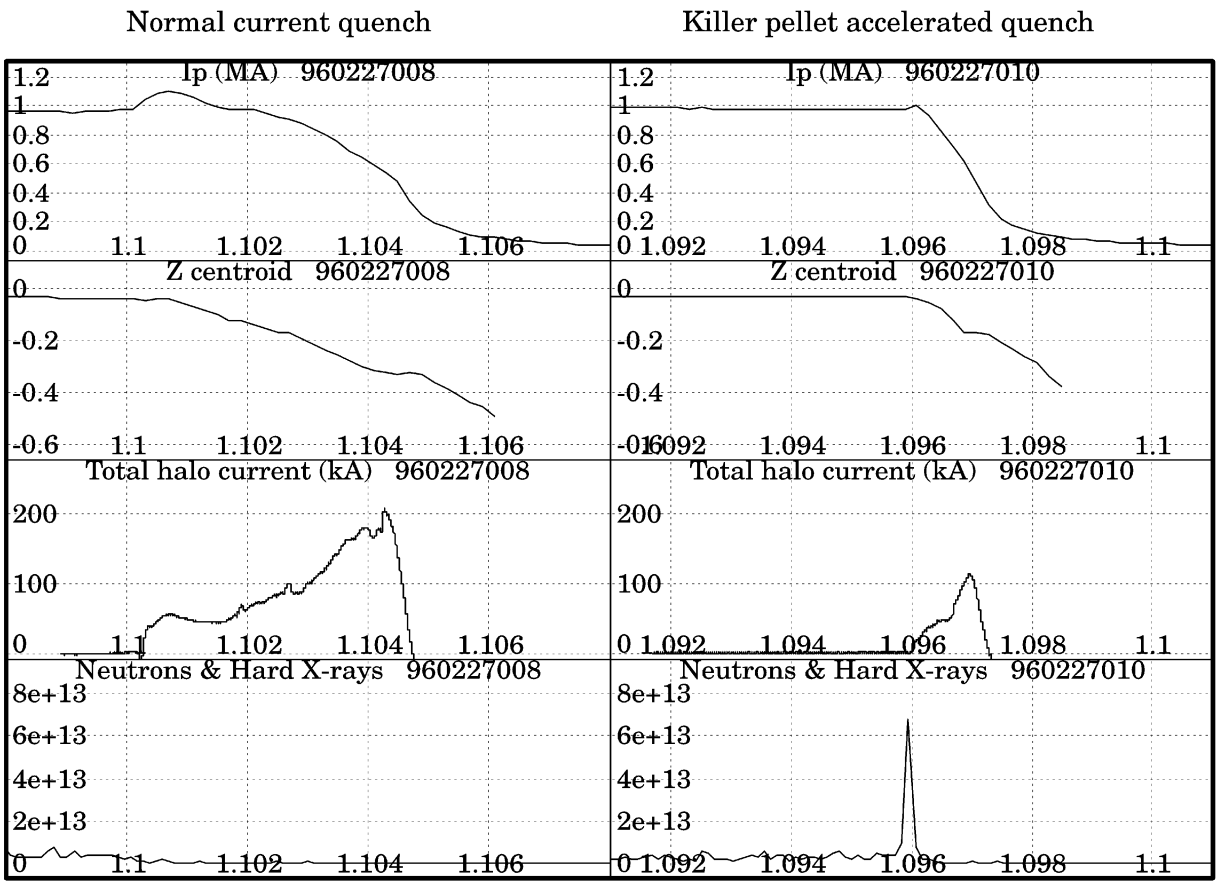

Fig. 13. Injection of pellets composed of high-*Z* material can mitigate disruption halo currents. Shown are the traces for a normal current quench (left) and a mitigated current quench (right).

gas jet system and fast imaging and NIMROD modeling of the three-dimensional magnetohydrodynamic physics involved in the disruption quench and halo current generation. These mitigation experiments are expected to verify whether or not such a scheme will be effective in ITER.

ACKNOWLEDGMENTS

Many remarkable engineers have contributed greatly to the design and fabrication of Alcator C-Mod, including R. Ballenger, M. Besen, J. Bosco, W. Burke, E. Byrne, H. Becker, G. Chikoski, R. Childs, W. Cochran, J. Daigle, G. Dekow, N. Diatchenko, S. Fairfax, C. Fertl, E. Fitzgerald, D. Griffen, S. Kochan, J. Minervini, B. Montgomery, J. Murphy, L. Myatt, M. Ohmstead, C. Park, W. Parkin, R. Pillsbury, N. Pierce, S. Rice, J. Rosati, J. Schultz, F. Silva, F. Tambini, D. Terry, E. Thibeault, P. Titus, F. Wong, and A. Zhukovsky. In addition, many physicists have made major contributions to the engineering effort, including P. Bonoli, R. Boivin, C. Fiore, J. Goetz, M. Greenwald, A. Hubbard, I. Hutchinson, B. Lipschultz, E. Marmar, R. Parker, M. Porkolab, J. Rice, Y. Takase, S. Wolfe, and S. Wukitch. Alcator C-Mod is supported by U.S. Department of Energy contract DE-FC02-99ER54512.

REFERENCES

1. S. FAIRFAX, *Proc. IEEE/NPSS 14th Symp. Fusion Engineering*, p. 656, IEEE (1991).

2. S. FAIRFAX, J. DAIGLE, V. BERTOLINO, J. PARANAY, and X. ZHONG, *Proc. IEEE/NPSS 15th Symp. Fusion Engineering*, p. 877, IEEE (1993).

3. W. BECK, *Proc. IEEE/NPSS 15th Symp. Fusion Engineering*, p. 292, IEEE (1993).

4. J. IRBY and R. GRANETZ, *Proc. IEEE/NPSS 17th Symp. Fusion Engineering*, p. 34, IEEE (1997).

5. I. H. HUTCHINSON et al., PFC/RR-88-11, MIT Plasma Science and Fusion Center (Aug. 1988).

6. S. WUKITCH et al., *Proc. IEEE/NPSS 19th Symp. Fusion Engineering*, p. 290, IEEE (2002).

7. G. TINIOS, PhD Thesis, Massachusetts Institute of Technology, Plasma Science and Fusion Center, RR 95-2 (1995).

8. I. H. HUTCHINSON, S. F. HORNE, G. TINIOS, S. M. WOLFE, and R. S. GRANETZ, *Fusion Technol.*, **30**, *2*, 137 (1996).

9. W. BECK, *Proc. IEEE/NPSS 15th Symp. Fusion Engineering*, p. 1121, IEEE (1993).

10. G. M. VOSS, Design Report F/MAST/35/T14, United Kingdom Atomic Energy Authority (May 1998).

11. I. H. HUTCHINSON, S. M. WOLFE, R. S. GRANETZ, J. E. RICE, A. E. HUBBARD, and J. IRBY, *Proc. 20th IAEA Fusion Energy Conf.*, EX/P5-6, International Atomic Energy Agency (2004).

12. S. M. WOLFE et al., *Phys. Plasmas*, **12**, 056110 (2005).

13. B. LaBOMBARD, B. LIPSCHULTZ, and S. KOCHAN, *Proc. IEEE/NPSS 14th Symp. Fusion Engineering*, p. 31, IEEE (1991).

14. J. ZAKS, M. DEMARIA, B. LaBOMBARD, R. GRANETZ, E. FITZGERALD, H. SAVELLI, and P. STAHLE, *Proc. IEEE/NPSS 19th Symp. Fusion Engineering*, p. 31, IEEE (2002).

15. P. TITUS et al., *Proc. IEEE/NPSS 19th Symp. Fusion Engineering*, p. 333, IEEE (2002).

16. P. TITUS, J. ZAKS, R. VIEIRA, D. GWINN, and B. LaBOMBARD, *Proc. IEEE/NPSS 21st Symp. Fusion Engineering*, IEEE (2005).

17. R. S. GRANETZ, J. IRBY, B. LaBOMBARD, Y. LIN, B. LIPSCHULTZ, and J. ZAKS, *Proc. IEEE/NPSS 21st Symp. Fusion Engineering*, IEEE (2005).

18. D. TERRY et al., *Proc. IEEE/NPSS 20th Symp. Fusion Engineering*, p. 524, IEEE (2003).

19. P. T. BONOLI et al., "Wave-Particle Studies in the Ion Cyclotron and Lower Hybrid Ranges of Frequencies in Alcator C-Mod," *Fusion Sci. Technol.*, **51**, 401 (2007).

20. J. A. STILLERMAN, M. FERRARA, T. W. FREDIAN, and S. M. WOLFE, *Fusion Eng. Des.*, **81**, 1905 (2006).

21. W. BURKE and E. BYRNE, *Proc. IEEE/NPSS 15th Symp. Fusion Engineering*, p. 786, IEEE (1993).

22. B. LIPSCHULTZ et al., *Phys. Plasmas*, **13**, 056117 (2006).

23. R. S. GRANETZ, I. H. HUTCHINSON, J. SORCI, J. H. IRBY, B. LaBOMBARD, and D. GWINN, *Nucl. Fusion*, **36**, 545 (1996).

24. ITER PHYSICS BASIS, Chap. 3, Sec. 4, *Nucl. Fusion*, **39**, 2321 (Dec. 1999).

25. R. YOSHINO, Y. NAKAMURA, and Y. NEYATANI, *Nucl. Fusion*, **36**, 295 (1996).

26. D. G. WHYTE et al., *Phys. Rev. Lett.*, **89**, 055001 (2002).